NMR Solution Structure of the Catalytic Fragment of Human Fibroblast Collagenase Complexed with a Sulfonamide Derivative of a Hydroxamic Acid Compound‡

Franklin J. Moy, Pranab K. Chanda,§ James M. Chen, Scott Cosmi,§ Wade Edris,§ Jerauld S. Skotnicki,|| Jim Wilhelm,§ and Robert Powers*

Department of Structural Biology, Department of Core Biotechnology and Department of Chemical Sciences, Wyeth-Ayerst Research, Pearl River, New York 10965

Received October 29, 1998; Revised Manuscript Received April 1, 1999

ABSTRACT: The solution structure of the catalytic fragment of human fibroblast collagenase (MMP-1) complexed with a sulfonamide derivative of a hydroxamic acid compound (CGS-27023A) has been determined using two-dimensional and three-dimensional heteronuclear NMR spectroscopy. The solution structure of the complex was calculated by means of hybrid distance geometry-simulated annealing using a combination of experimental NMR restraints obtained from the previous refinement of the inhibitor-free MMP-1 (*1*) and recent restraints for the MMP-1:CGS-27023A complex. The hydroxamic acid moiety of CGS-27023A was found to chelate to the "right" of the catalytic zinc where the *p*-methoxyphenyl sits in the S1′ active-site pocket, the isopropyl group is in contact with H83 and N80, and the pyridine ring is solvent exposed. The sulfonyl oxygens are in hydrogen-bonding distance to the backbone NHs of L81 and A82. This is similar to the conformation determined by NMR of the inhibitor bound to stromelysin (*2, 3*). A total of 48 distance restraints were observed between MMP-1 and CGS-27023A from 3D ^{13}C-edited/^{12}C-filtered NOESY and 3D ^{15}N-edited NOESY experiments. An additional 18 intramolecular restraints were observed for CGS-27023A from a 2D ^{12}C-filtered NOESY experiment. A minimal set of NMR experiments in combination with the free MMP-1 assignments were used to assign the MMP-1 ^{1}H, ^{13}C, and ^{15}N resonances in the MMP-1:CGS-27023A complex. The assignments of CGS-27023A in the complex were obtained from 2D ^{12}C-filtered NOESY and 2D ^{12}C-filtered TOCSY experiments.

The rational design of protein inhibitors based on structural information has proven to be an extremely valuable method for drug development as evident from the recent success with HIV protease inhibitors (*4*−*6*). A fundamental component of the structure-based approach to drug development is the iterative refinement of a novel inhibitor through a succession of protein-inhibitor structures (*7*−*9*). This necessitates a relatively high-throughput of the structure determination process for each new protein−inhibitor complex by either NMR[1] or X-ray methodology. A rapid approach for NMR structure determination utilizes X-nucleus filtered multidimensional experiments in conjunction with a refined structure of the target protein to solve the structure of the complex (*10*). Previously, we presented the near complete ^{1}H, ^{15}N, ^{13}CO, and ^{13}C assignments, solution secondary structure, and dynamics for MMP-1 (*11*) and the refinement of a high-resolution solution structure of inhibitor-free MMP-1 (*1*). These results provide the initial framework for such a structure-based drug development program. In this paper, we present the determination of the solution conformation of MMP-1 complexed with a sulfonamide derivative of a hydroxamic acid compound (CGS-27023A).

The matrix metalloproteinase (MMP) family is a highly active set of targets for the design of therapeutic agents for the disease areas of arthritis and oncology (for reviews, see refs *12*−*16*). The MMPs are involved in the remodeling and degradation of extracellular matrix proteins and are highly regulated. The apparent loss in this regulation results in the pathological destruction of connective tissue and the ensuing disease state. There have been a number of X-ray and NMR structures solved for the catalytic domain of MMPs complexed with a variety of inhibitors (*2, 17*−*28*), a crystal structure of collagenase complexed to itself (*29*), and an NMR structure of inhibitor-free MMP-1 (*1*).

There is a relatively high sequence homology (>40%) in the catalytic domain between members of the MMP family resulting in a close similarity in the overall three-dimensional

‡ Atomic coordinates for the 30 final simulated annealing structures (3AYK) and the restrained minimized mean structure (4AYK) of MMP-1 complexed with CGS-27023A have been deposited in the Brookhaven Protein Data Bank.

* To whom correspondence should be addressed.

§ Department of Core Biotechnology.

|| Department of Chemical Sciences.

[1] Abbreviations: MMP-1, matrix metalloproteinase-1; DTT, DL-1,4-dithiothreitol; NMR, nuclear magnetic resonance; 2D, two-dimensional; 3D, three-dimensional; HSQC, heteronuclear single-quantum coherence spectroscopy; HMQC, heteronuclear multiple-quantum coherence spectroscopy; TPPI, time-proportional phase incrementation; NOE, nuclear Overhauser effect; NOESY, nuclear Overhauser enhanced spectroscopy; TOCSY, total correlated spectroscopy; COSY, correlated spectroscopy; CBCA(CO)NH; Cβ to Cα to amide proton to nitrogen (via carbonyl); C(CO)NH, carbon to amide proton to nitrogen (via carbonyl); HNHA, amide proton to nitrogen to CαH proton and HNCA, amide proton to nitrogen to α-carbon correlation.

10.1021/bi982576v CCC: $18.00
Published on Web 05/14/1999

fold for these proteins. Despite this overall structural similarity, there exists distinct substrate specificity between these enzymes, particularly between the three major classes: collagenases, stromelysins, and gelatinases. The most distinct structural difference between the MMPs is the relative size and shape of the S1′ pocket. Additionally, there are some critical residue differences between the MMPs in the active site which may also contribute to substrate selectivity. In addition to using the structural information for designing potent inhibitors to the MMPs, there may be a benefit in designing selectivity between the various subtypes (*30*−*34*). Since an NMR structure of stromelysin complexed with CGS-27023A has been previously reported (*2, 3*), the structure of MMP-1 complexed with CGS-27023A reported in this manuscript provides a unique structural comparison of a biologically active nonpeptidic inhibitor bound to two related MMPs.

MATERIALS AND METHOD

CGS-27023A Synthesis. A sulfonamide derivative of a hydroxamic acid compound**,** CGS-27023A, was prepared according to the literature procedure (*35*). Thus, the sulfonamide derived from D-valine and *p*-methoxyphenylsulfonyl chloride was converted to the *tert*-butyl ester. Alkylation with 3-picolyl chloride and removal of the *tert*-butyl ester (HCl/dioxane) afforded the corresponding acid. The hydroxamic acid was formed via the carbodiimde procedure (EDC/HOBT/NMM, then *tert*-butylhydroxylamine). Removal of the *tert*-butyl protecting group (HCl/EtOH) and conversion to the HCl salt yielded CGS-27023A.

NMR Sample Preparation. Uniformly (>95%) ^{15}N- and ^{15}N/^{13}C-labeled human recombinant MMP-1 was expressed in *Escherichia coli* and purified as described previously (*11, 20*) except that anion exchange was carried out on Source 30Q anion-exchange resin (Pharmacia, Piscataway, NJ).

The MMP-1:CGS-27023A NMR sample contained 1 mM ^{15}N- or ^{15}N/^{13}C-labeled MMP-1 with CGS-27023A in a 1:1 ratio. The sample was prepared by repeated buffer exchange using 20−30 mL of solution containing 10 mM deuterated Tris-Base, 100 mM NaCl, 5 mM $CaCl_2$, 0.1 mM $ZnCl_2$, 2 mM NaN_3, 10 mM deuterated DTT, and 0.2 mM CGS-27023A in either 90% H_2O/10% D_2O or 100% D_2O. Buffer exchange was carried out on a Millipore Ultrafree-15 Centrifugal Filter Unit. Excess CGS-27023A was removed by additional buffer exchanges where CGS-27023A was removed from the buffer.

NMR Data Collection. All spectra were recorded at 35 °C on a Bruker AMX600 spectrometer using a gradient enhanced triple-resonance ^{1}H/^{13}C/^{15}N probe. For spectra recorded in H_2O, water suppression was achieved with the WATERGATE sequence and water-flip back pulses (*36, 37*). Quadrature detection in the indirectly detected dimensions were recorded with States-TPPI hypercomplex phase incrementation (*38*). Spectra were collected with appropriate refocusing delays to allow for 0,0 or −90,180 phase correction.

The assignments of the ^{1}H, ^{15}N, and ^{13}C resonances of MMP-1 in the MMP-1:CGS-27023A complex were based on a minimal set of experiments: 2D ^{1}H-^{15}N HSQC, 3D ^{15}N-edited NOESY (*39, 40*), CBCA(CO)NH (*41*), C(CO)NH (*42*), HNHA (*43*), and HNCA (*44*). The acquisition parameters for each of the experiments used in determining the solution structure of the MMP-1:CGS-27023A complex were as reported previously (*45*).

The resonance assignments and bound conformation of CGS-27023A in the MMP-1:CGS-27023A complex were based on the 2D ^{12}C/^{12}C-filtered NOESY (*46, 47*), 2D ^{12}C/^{12}C-filtered TOCSY (*46, 47*), and ^{12}C/^{12}C-filtered COSY experiments (*48*).

The 2D ^{12}C/^{12}C-filtered COSY and 2D ^{12}C/^{12}C-filtered TOCSY spectra were recorded with 512 complex points in t_1, 2048 real points in t_2, and 64 scans/increments. The 2D ^{12}C/^{12}C-filtered NOESY spectra were recorded with 256 complex points in t_1, 2048 real points in t_2, and 128 scans/increment. Spectra windows for all 2D isotope-filtered experiments were 8064.5 Hz in both dimensions with the carrier at 4.75 ppm.

The MMP-1:CGS-27023A structure is based on observed NOEs from the 3D ^{15}N-edited NOESY (*39, 40*), 3D ^{13}C-edited/^{12}C-filtered NOESY (*49*), and $^3J_{NH\alpha}$ coupling constants measured from the relative intensity of Hα cross-peaks to the NH diagonal in the HNHA experiment (*43*). The 3D ^{15}N-edited NOESY and 3D ^{13}C-edited/^{12}C-filtered NOESY experiments were collected with 100 ms and (50−110) ms mixing times, respectively. The 3D ^{13}C-edited/^{12}C-filtered NOESY spectrum was recorded with 32 transients/increment with 26, 84, and 512 complex points in t_1 (^{13}C), t_2 (^{1}H), and t_3 (^{1}H), respectively. Carrier positions in ^{1}H and ^{13}C are at 4.75 and 43 ppm, respectively. The spectrum windows are 3600, 5040, and 8064.5 Hz in t_1 (^{13}C), t_2 (^{1}H), and t_3 (^{1}H), respectively. The acquisition parameters of all other experiments for MMP-1 with CGS-27023A were identical to parameters reported previously for free MMP-1 (*1*).

Spectra were processed using the NMRPipe software package (*50*) and analyzed with PIPP (*51*) on a Sun Sparc Workstation. When appropriate, data processing included a solvent filter, zero-padding data to a power of 2, linear predicting back one data point of indirectly acquired data to obtain zero phase corrections, linear prediction of additional points for the indirectly acquired dimensions to increase resolution. Linear prediction by the means of the mirror image technique was used only for constant-time experiments (*52*). In all cases, data was processed with a skewed sine-bell apodization function and one zero-filling was used in all dimensions.

Interproton Distance Restraints. The NOEs assigned from 3D ^{13}C-edited/^{12}C-filtered NOESY and 3D ^{15}N-edited NOESY experiments were classified into strong, medium, and weak, corresponding to interproton distance restraints of 1.8−2.7 Å (1.8−2.9 Å for NOEs involving NH protons), 1.8−3.3 Å (1.8−3.5 Å for NOEs involving NH protons), and 1.8−5.0 Å, respectively (*53, 54*). Upper distance limits for distances involving methyl protons and nonstereospecifically assigned methylene protons were corrected appropriately for center averaging (*55*).

Structure Calculations. The structures were calculated using the hybrid distance geometry-dynamical simulated annealing method of Nilges et al. (1988) (*56*) with minor modifications (*57*) using the program XPLOR (*58*), adapted to incorporate pseudopotentials for $^3J_{NH\alpha}$ coupling constants (*59*), secondary ^{13}Cα/^{13}Cβ chemical shift restraints (*60*), and a conformational database potential (*61, 62*). The target function that is minimized during restrained minimization

and simulated annealing comprises only quadratic harmonic terms for covalent geometry, $^3J_{NH\alpha}$ coupling constants, and secondary $^{13}C\alpha/^{13}C\beta$ chemical shift restraints, square-well quadratic potentials for the experimental distance and torsion angle restraints, and a quartic van der Waals term for nonbonded contacts. All peptide bonds were constrained to be planar and trans. There were no hydrogen-bonding, electrostatic, or 6-12 Lennard-Jones empirical potential energy terms in the target function.

The restraints used for the refinement of the inhibitor-free MMP-1 NMR structure (*1*) were amended with the 48 distance restraints observed between MMP-1 and CGS-27023A from the 3D ^{13}C-edited/^{12}C-filtered NOESY and 3D ^{15}N-edited NOESY experiments and the 18 intramolecular restraints observed for CGS-27023A from the 2D ^{12}C-filtered NOESY experiment. The inhibitor-free MMP-1 NMR restraints were modified as appropriate for residues in the vicinity of the active site (80−83, 114−119, and 136−142) by either removing restraints inconsistent with the MMP-1:CGS-27023A structure and/or by the addition of new restraints observed in the complex. Additionally, the MMP-1:CGS-27023A complex was refined using the $^3J_{NH\alpha}$ coupling constants determined from the HNHA (*43*) experiment and secondary $^{13}C\alpha/^{13}C\beta$ chemical shift restraints from the assignments for the complex.

The bound conformation for CGS-27023A was generated using QUANTA97 and CHARMM (Molecular Simulations Inc., San Diego), and the XPLOR topology and parameter files were generated using XPLOR2D (*63*). Generation of the bound conformation of CGS-27023A is described in the following general procedure. The initial CGS-27023A structure was created using the QUANTA97 2D-sketcher application and was subjected to 500 steps of CHARMM minimization. This was followed by an additional 500 steps of restrained minimization using the 18 intramolecular CGS-27023A NOE restraints with the NOE scaling factor set to 500.

The starting MMP-1:CGS-27023A complex structure for the simulated-annealing protocol was then obtained by manually docking the bound conformation of CGS-27023A into the restrained minimized average structure previously determined for the inhibitor-free catalytic domain of MMP-1 (*1*). CGS-27023A was then subjected to 1000 steps of CHARMM minimization with the 18 intramolecular NOE restraints where the coordinates for MMP-1 were kept fixed. The structure was then further minimized with both the 18 intramolecular CGS-27023A restraints and the 48 distance restraints observed between MMP-1 and CGS-27023A while keeping the MMP-1 coordinates fixed. This approach approximated the positioning of CGS-27023A in the active site of MMP-1 without distorting the MMP-1 structure. The final structure was exported as a PDB file and used as the starting point for XPLOR simulated annealing protocol where all the residues in the structure were free to move. Since the initial stage of the simulated annealing protocol corresponds to high-temperature dynamics (1500 K) with a relatively weak XPLOR NOE force constant (2), the initial MMP-1:CGS-27023A structure does not bias the structure determination process since the structure is effectively free to explore the available conformational space. Additionally, each iteration of the simulated annealing process begins with a random trajectory for the molecular dynamics. The fact that these trajectories differ by upward of 10 Å ensures a distinct exploration of conformational space for the ensemble of MMP-1:CGS-27023A structures determined from the simulated annealing protocol.

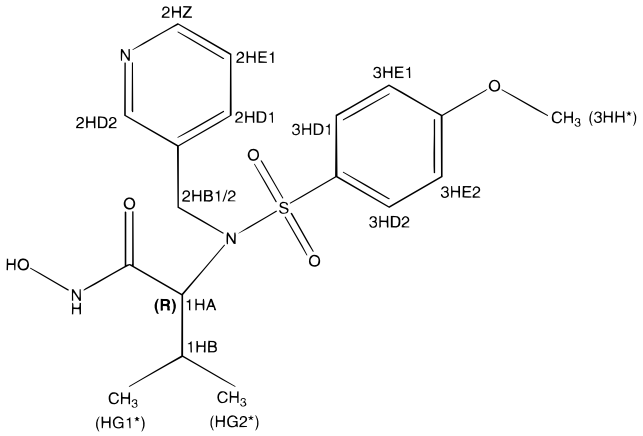

FIGURE 1: Illustration of the sulfonamide derivative of the hydroxamic acid inhibitor (CGS-27023A) with the corresponding proton labels.

Computer Models of MMP Complexed to CGS-27023A. Molecular modeling was carried out using the Sybyl molecular modeling package from Tripos, Inc. (St. Louis, MO) on a Silicon Graphics Inc. Indigo II. The matrilysin (MMP-7:1MMR), neutrophil collagenase (MMP-8:1MNC) and stromelysin (MMP-3:2SRT) complexes were used for developing the molecular model of inhibitor CGS-27023A bound to the enzymes (*18, 21, 64*). Since the coordinates for the stromelysin:CGS-27023A complex were not yet available (*2, 3*), the CGS-27023A inhibitor was merged into the active site cavity of each of the available MMPs based on the protein overlaps as depicted in Figure 6A. According to the published structural descriptions of the protein inhibitor interactions (*2, 3*), a set of nested energy refinement procedures (*9, 65*) was used for optimizing the modeled complexes of the MMPs bound to the inhibitor. The protein superpositions were generated based on a rigid body fit minimizing the root-mean-square deviations between the backbone atoms of all the proteins. The S1′ pockets described within were represented as Connolly solvent accessible surfaces and generated with the MOLCAD algorithm from Tripos, Inc. using a 1.4 Å water probe.

RESULTS AND DISCUSSION

CGS-27023A Resonance Assignments and Bound Conformation. The primary structure of CGS-27023A along with the proton naming convention consistent with Gonnella et al. (1997) is shown in Figure 1. The MMP-1:CGS-27023A NMR sample was composed of $^{13}C/^{15}N$ labeled MMP-1 and unlabeled CGS-27023A. Thus, traditional 2D-NOESY, COSY, and TOCSY spectra of CGS-27023A in the presence of MMP-1 were determined from 2D ^{12}C-filtering experiments (*46*−*48*) where only cross-peaks between protons attached to ^{12}C carbons are observed. These experiments efficiently filter all protein resonances and allow for the straightforward analysis of the CGS-27023A spectrum. Chemical shift assignments for CGS-27023A complexed with MMP-1 along with the previously reported assignments for free CGS-27023A and CGS-27023A bound to stromelysin (*2*) are listed in Table 1. It is interesting to note that while the observed

Table 1: Chemical Shifts of CGS-27023A

proton	MMP-1 (ppm)	stromelysin[a] (ppm)	free[a] (ppm)
1HA	4.59	4.55	3.94
1HB	2.30	2.36	2.11
HG1*	0.89	0.87	0.79
HG2*	0.98	1.08	0.79
2HB1	5.20	4.97	4.74
2HB2	5.20	4.53	4.74
2HD1	8.22	8.19	7.68
2HE1	7.62	7.51	7.28
2HZ	8.60	8.53	8.33
2HD2	8.68	8.59	8.32
3HD1/2	7.88	7.71	7.52
3HE1/2	7.05	6.96	6.95
3HH*	4.05	3.96	3.83

[a] Chemical shifts as reported by Gonnella et al. (1997).

Table 2: Observed NOEs for the Bound Conformation of CGS-27023A

CGS-27023A	NOE class	CGS-27023A	NOE class
HG1*−1HB	M	1HB-2HD2	W
HG1*−1HA	S	3HH*−3HE2	M
HG1*−2HB1/2	W	3HH*−3HD2	W
HG1*−3HD1	W	1HA-2HB1/2	M
HG1*−2HE1	W	1HA-3HD1	M
HG1*−2HD1	W	1HA-2HD2	W
HG1*−2HZ	W	2HB1/2−3HD2	W
HG1*−2HD2	W	2HB1/2−2HD2	W
HG2*−1HB	M	3HE1/2−3HD1/2	S
HG2*−1HA	S	2HE1−2HD1	S
HG2*−2HD2	W	2HE1−2HZ	M
1HB-1HA	W	2HD1−2HZ	W
1HB-2HB1/2	W		

chemical shifts for CGS-27023A in MMP-1 and stromelysin are comparable (accounting for the slight pH difference of 6.5 in MMP-1 and 6.8 in stromelysin), there are some significant differences. Particularly, two distinct resonances were observed for 2HB1 and 2HB2 in stromelysin compared to a single resonance in MMP-1, which is shifted 0.23 and 0.67 ppm downfield relative to stromelysin. Additionally, the two methyl groups in the isopropyl moiety have a smaller chemical shift dispersion in MMP-1 (0.09 ppm) compared to stromelysin (0.21 ppm). These results imply a different environment for these resonances in MMP-1 and stromelysin. Consistent with the stromelysin assignments was the observation that the protons on the *p*-methoxyphenyl ring are degenerate suggesting rapid ring flips when complexed to either MMP-1 or stromelysin.

CGS-27023A does not adopt a preferred conformation in the absence of MMP-1 as evident by the lack of structural NOEs. Therefore, the observed NOEs and conformation of CGS-27023A in the presence of MMP-1 is strictly a result of the binding of CGS-27023A to MMP-1. The observed intramolecular NOEs for CGS-27023A bound to MMP-1 were obtained from the 2D ^{12}C-filtered NOESY spectra and are listed in Table 2. A number of the observed NOEs correspond to a sequential interaction which have no effect on the overall conformation of the inhibitor and were not used in the refinement of CGS-27023A or the complex. The weak NOE between 1HA and 2HD2 was attributed to spin diffusion since HG1* is positioned between 1HA and 2HD2 and cannot be accommodated for in the bound conformation. This was confirmed from the relative intensity of this NOE in the 50 and 100 ms mixing time NOESY. A stereoview of the bound conformation of CGS-27023A is shown in Figure 2.

Previous to our solution of the conformation of CGS-27023A bound to MMP-1, Gonnella et al. (1995) published the bound conformation of two similar analogues (I-1 and I-2) of CGS-27023A bound to stromelysin using transfer NOEs. A distinct feature of I-2 was the base stacking of the *p*-methoxyphenyl ring and the pyridyl ring as evident by TR-NOEs between the two aromatic rings. This stacked ring conformation is clearly distinct from the "splayed" ring conformation observed for CGS-27023A bound to MMP-1 (Figure 2). This "splayed" conformation for CGS-27023A is consistent with the lack of any observable NOEs between the two aromatic ring systems while being consistent with the NOE between 2HB1/2 and 3HD2. Another distinct feature of the CGS-27023A "splayed" conformation is the proximity of a single methyl from the isopropyl moiety to both the pyridyl and *p*-methoxyphenyl rings. This is consistent with the observation of a number of aromatic NOEs to only one methyl group in the 2D ^{12}C-filtered NOESY spectra (Table 2).

Resonance Assignments for MMP-1 in the Complex. The nearly complete resonance assignments for inhibitor-free MMP-1 (*11*) provided the starting point for the assignments of MMP-1 in the complex. Three important observations

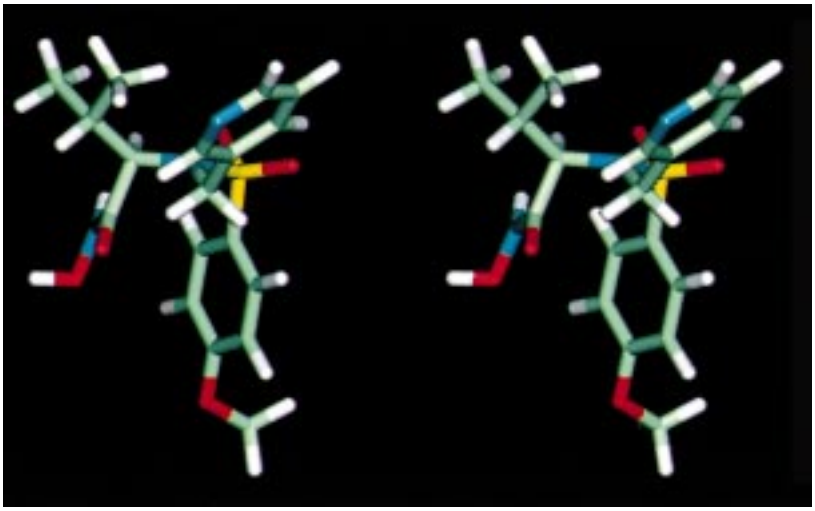

FIGURE 2: Cross-eyed stereoview of the MMP-1 bound conformation of CGS-27023A.

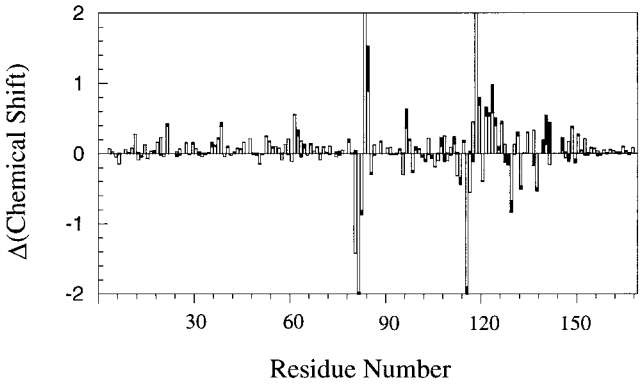

FIGURE 3: Plot of the MMP-1 NH (■) and ^{15}N (□) chemical shift perturbations (ppm) per residue upon binding CGS-27023A. For clarity, the scale of the *y*-axis has been reduced resulting in the chemical shift perturbations for a few residues being off-scale.

facilitated these assignments and suggested a simple "bootstrap" approach using a minimal set of NMR experiments. First, as apparent by the chemical shift perturbations in the 2D ^{1}H-^{15}N HSQC spectra (Figure 3), >90% of the MMP-1 residues was not perturbed by the presence of CGS-27023A. This indicates that the majority of the MMP-1 structure is unaffected and that only residues 80−85, 112−124, and 134−143, which are in close proximity to CGS-27023A, incur a chemical shift change. Therefore, the backbone assignments of residues in the vicinity of CGS-27023A were obtained by following sequential NOE connectivities in the 3D ^{15}N-edited NOESY spectra by starting with unaffected residues sequential to perturbed residues. The simplest approach was to follow sequential NH−NH NOEs by using the symmetry function in PIPP (*51*).

Second, while significant ^{1}H and ^{15}N chemical shift perturbations occur for residues in the vicinity of CGS-27023A, the general NOE pattern is intact. Simple comparison of the 3D ^{15}N-edited NOESY spectra of the inhibitor-free MMP-1 and MMP-1:CGS-27023A readily identifies the sequential and intraresidue NOEs in the MMP-1:CGS-27023A spectra (Figure 4). Thus, the assignments were further confirmed by the presence of additional sequential NOE cross-peaks such as NH-Hα and NH−Hβ NOEs. Additionally, this provided a straightforward approach to side-chain ^{1}H assignments.

Third, ^{13}C chemical shifts did not incur any significant chemical shift perturbation even for residues in close proximity to CGS-27023A. While the NOE patterns in the 3D ^{15}N-edited NOESY spectra were sufficient to assign all the residues perturbed by CGS-27023A, additional conformation of the assignments was obtained from proper connectivity in the HNCA and CBCA(CO)NH experiments and from the proper spin systems in the C(CO)NH experiments. These data established the observation that the ^{13}C resonances in the MMP-1:CGS-27023A complex were essentially identical to the inhibitor-free MMP-1 assignments.

Structure Determination. The refinement of the solution structure of MMP-1:CGS-27023A was based on distance and dihedral restraints determined for the high-resolution solution structure of inhibitor-free MMP-1 appended with the intra- and intermolecular NOEs from the MMP-1:CGS-27023A complex. The inhibitor-free MMP-1 NMR restraints were modified as appropriate for residues in the vicinity of the active site (80−83, 114−119, and 136−142) by either

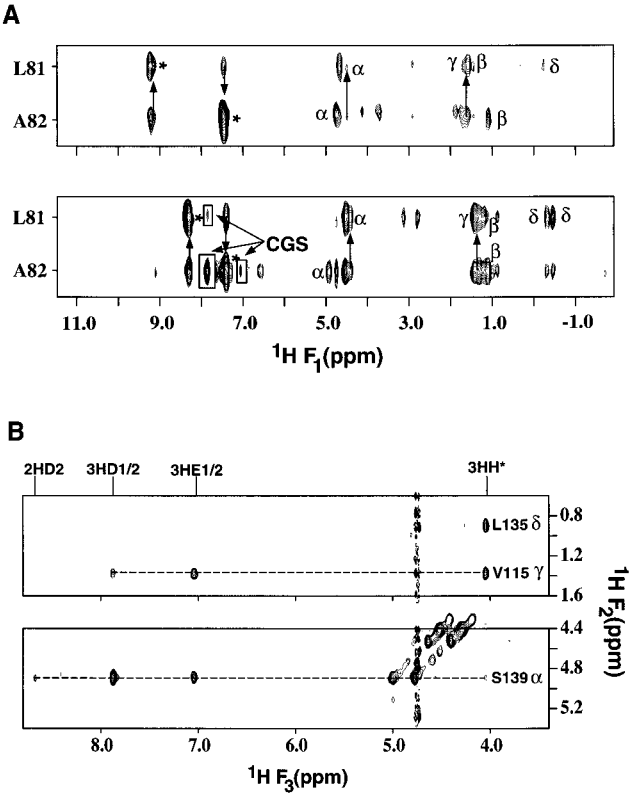

FIGURE 4: (A) Amide strips taken from the 3D ^{15}N-edited NOESY−HSQC spectrum of (top) inhibitor-free MMP-1 and (bottom) MMP-1:CGS-27023A for L81 and A82. The intermolecular NOEs between MMP-1 and CGS-27023A are boxed and labeled. The diagonal peaks are indicated by an asterisk. Intraresidue Hα-NH, Hβ-NH, Hγ-NH, and Hδ-NH are labeled. Sequential NOEs are indicated by a solid arrow. (B) Two expanded regions from two different ^{13}C (F1) planes corresponding to L135δ/V115γ and S139α of the ^{13}C-edited/^{12}C-filtered NOESY spectrum. The CGS-27023A resonances are labeled and NOEs from a single residue are connected by a dotted line.

removing restraints inconsistent with the MMP-1:CGS-27023A structure and/or by the addition of new restraints observed in the complex. Inhibitor-free MMP-1 NMR restraints were identified as inconsistent with the MMP-1:CGS-27023A structure when the restraint was consistently violated in structures calculated for the complex. Since the restraints from the inhibitor-free MMP-1 structure determination did not exhibit any distance violations greater than 0.1 Å or dihedral angle violations greater than 1°, any observed violation with the MMP-1:CGS-27023A structure was inherently incompatible with the new complex and generally violated in most if not all the calculated structures. This technique effectively filters out any bias in the structure determination process for the complex by giving the NOEs observed for the MMP-1:CGS-27023A absolute precedent over the inhibitor-free MMP-1 restraints. This method permitted the structure of the active site of MMP-1 to be determined primarily by the observed intermolecular NOEs between MMP-1 and CGS-27023A and the CGS-27023A intramolecular NOEs while the remainder of the protein is predominately defined by the inhibitor-free MMP-1 restraints. These results are consistent with the observation that the conformation of residues distal to the active site were unchanged in the complex since chemical shifts for these residues are essentially identical between the free and complexed form of MMP-1.

Table 3: Structural Statistics and Atomic rms Differences[a]

A. Structural Statistics

	⟨SA⟩	$(\overline{SA})_r$	$(\overline{SA})_{rfree}$[b]
rms deviations from experimental distance restraints (Å)[c]			
all (2482)	0.015 ± 0.002	0.015	0.014
interresidue sequential ($\|i-j\|=1$) (686)	0.008 ± 0.004	0.007	0.011
interresidue short range ($1<\|i-j\|\le 5$) (472)	0.012 ± 0.003	0.017	0.013
interresidue long-range ($\|i-j\|>5$) (637)	0.013 ± 0.002	0.018	0.017
intraresidue (537)	0.006 ± 0.006	0.001	0.000
H bonds (84)[d]	0.035 ± 0.006	0.027	0.034
CGS-27023A (66)	0.045 ± 0.007	0.032	
rms deviation from exptl dihedral restraints (deg) (425)[c,e]	0.225 ± 0.040	0.258	0.137
rms deviation from exptl Cα restraints (ppm) (135)	1.11 ± 0.02	1.11	1.09
rms deviation from exptl Cβ restraints (ppm) (115)	1.06 ± 0.03	1.07	1.06
rms deviation from $^3J_{NH\alpha}$ restraints (Hz) (118)	0.73 ± 0.03	0.64	1.15
F_{NOE} (kcal mol^{-1})[f]	26.2 ± 9.4	25.9	22.2
F_{tor} (kcal mol^{-1})[f]	1.29 ± 0.46	1.65	0.46
F_{repel} (kcal mol^{-1})[f]	26.1 ± 2.3	83.8	100.5
F_{L-J} (kcal mol^{-1})[g]	−688 ± 13	−625	−616
deviations from idealized covalent geometry			
bonds (Å) (2604)	0.005 ± 0	0.003	0.003
angles (deg) (4669)	0.469 ± 0.015	0.443	0.488
impropers (deg) (1434)[h]	0.398 ± 0.035	0.326	0.364
PROCHECK[i]			
overall G-factor	0.21 ± 0.01	0.29	0.28
residues in most favorable region of Ramachandran plot	90.6 ± 1.0	89.9	89.9
H-bond energy	0.77 ± 0.05	0.90	0.90
no. of bad contacts/100 residues	4.5 ± 1.0	1.9	4.5

B. Atomic rms Differences (Å)

		active-site residues[l]		residues 7−137, 145−163		secondary structure[m]		ordered side chain[n];
	CGS-27023A[k]	backbone	all	backbone	all	backbone	all	all
⟨SA⟩ vs $\overline{SA}$	0.28 ± 0.08	0.54 ± 0.03	0.92 ± 0.17	0.43 ± 0.03	0.80 ± 0.04	0.29 ± 0.04	0.64 ± 0.06	0.53 ± 0.03
⟨SA⟩ vs $(\overline{SA})_r$	0.34 ± 0.12	0.60 ± 0.13	1.01 ± 0.17	0.45 ± 0.04	0.88 ± 0.05	0.31 ± 0.04	0.71 ± 0.07	0.58 ± 0.04
$(\overline{SA})_r$ vs $\overline{SA}$	0.20	0.27	0.44	0.14	0.37	0.10	0.32	0.23
$\overline{SA}$ vs $(SA)_{rfree}$		0.91	1.27	0.51	0.75	0.31	0.52	0.60
$(\overline{SA})_r$ vs $(\overline{SA})_{rfree}$		1.00	1.31	0.48	0.75	0.31	0.56	0.60
⟨SA⟩ vs $(\overline{SA})_{rfree}$		1.05 ± 0.17	1.55 ± 0.25	0.66 ± 0.08	1.09 ± 0.06	0.43 ± 0.05	0.82 ± 0.07	0.80 ± 0.07

[a] The notation of the structures is as follows: ⟨SA⟩ are the final 30 simulated annealing structures; $\overline{SA}$ is the mean structure obtained by averaging the coordinates of the individual SA structures best fit to each other (excluding residues 1−6, 138−144, and 164−169); and $(\overline{SA})_r$ is the restrained minimized mean structure (residues 7−163) obtained by restrained minimization of the mean structure $\overline{SA}$ (*56*). The number of terms for the various restraints is given in parentheses. [b]The inhibitor-free MMP-1 restrained minimized mean structure (residues 7−163) previously determinied by NMR (*1*). [c]None of the structures exhibited distance violations greater than 0.1 Å or dihedral angle violations greater than 1°. [d]For backbone NH−CO hydrogen bond there are two restraints: r_{NH-O} = 1.5−2.3 Å and r_{N-O} = 2.5−3.3 Å. All hydrogen bonds involve slowly exchanging NH protons. [e]The torsion angle restraints comprise 155 ϕ, 134 ψ, 102 χ1, and 34 χ2 restraints. [f]The values of the square-well NOE (F_{NOE}) and torsion angle (F_{tor}) potentials (cf. eqs 2 and 3 in ref *54*) are calculated with force constants of 50 kcal mol^{-1} Å^{-2} and 200 kcal mol^{-1} rad^{-2}, respectively. The value of the quartic van der Waals repulsion term (F_{rep}) (cf. eq 5 in ref *56*) is calculated with a force constant of 4 kcal mol^{-1} Å^{-4} with the hard-sphere van der Waals radius set to 0.8 times the standard values used in the CHARMM (*67*) empirical energy function (*56, 68, 69*). [g]E_{L-J} is the Lennard-Jones-van der Waals energy calculated with the CHARMM emperical energy function and is *not* included in the target function for simulated annealing or restrained minimization. [h]The improper torsion restraints serve to maintain planarity and chirality. [i]These were calculated using the PROCHECK program (*70*). [k]Only heavy atoms from the CGS-27023A structure were used for the rms calculation. [l]The residues in the active site correspond to 80−85, 112−124, and 134−143. [m]The residues in the regular secondary structure are 13−19 (β_1), 48−53(β_2), 59−65(β_3), 82−85(β_4), 94−99(β_5), 27−43(α_1), 112−124(α_2), and 150−160(α_3). [n]The disordered side-chains that were excluded are as follows: residues 1−6; residues 138−144; residues 164−169; Arg 8 from Cδ; Glu 10 from Cδ; Gln 11 from Cδ; Arg 17 beyond Cδ; Glu 19 from Cδ; Asn 20 from Cγ; Asp 24 from Cγ; Arg 27 beyond Cδ; Asp 31 from Cγ; Glu 35 from Cδ; Lys 36 from Cϵ; Gln 39 from Cδ; Asn 43 beyond Cγ; Lys 51 from Cϵ; Glu 54 from Cγ; Gln 56 from Cδ; Arg 65 beyond Cδ; Asp 70 from Cγ; Asn 71 from Cγ; Asp 75 from Cγ; Gln 86 from Cδ; Glu 99 from Cδ; Glu 101 from Cδ; Arg 102 beyond Cδ; Asn 105 beyond Cδ; Phe 107 from Cγ; Argl 108 beyond Cδ; Glu 109 from Cδ; Asn 111 from Cγ; Arg 114 beyond Cδ; Glu 119 from Cδ; Ser 123 beyond Cβ; Ile 132 from Cγ; Asp 145 from Cβ; Gln 147 from Cδ; Gln 150 from Cδ; Gln 157 from Cδ; and Arg 162 beyond Cδ.

The final 30 simulated annealing structures were calculated on the basis of 3275 experimental NMR restraints consisting of 2482 approximate interproton distance restraints, 84 distance restraints for 42 backbone hydrogen bonds, 425 torsion angle restraints comprised of 155 ϕ, 134 Ψ, 102 χ_1 and 34 χ_2 torsion angle restraints, 118 $^3J_{NH\alpha}$ restraints, and 135 Cα and 115 Cβ chemical shift restraints. A summary of the structural statistics for the final 30 simulated annealing (SA) structures of human MMP-1 in the MMP-1:CGS-27023A complex is provided in Table 3 and the restrained minimized average solution structure of the MMP-1:CGS-27023A complex is shown in Figure 5A. The atomic rms distribution of the 30 simulated annealing structures about the mean coordinate positions for residues 7−137 and 145−163 is 0.43 ± 0.03 Å for the backbone atoms, 0.80 ± 0.04 Å for all atoms, and 0.53 ± 0.03 Å for all atoms excluding

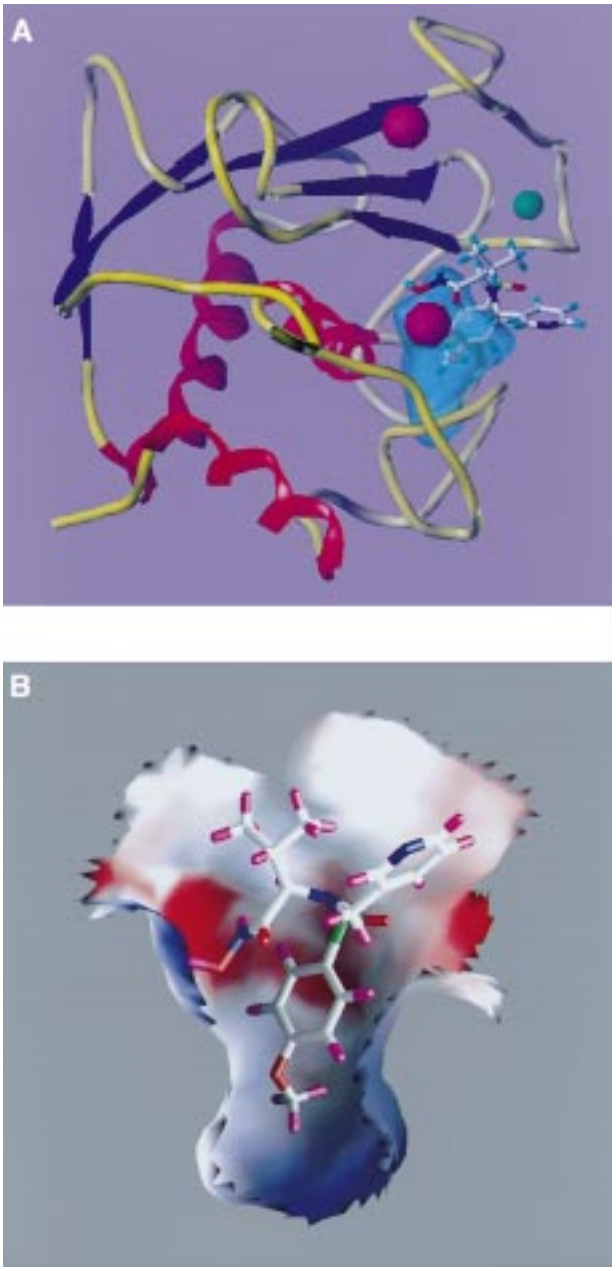

FIGURE 5: (A) Ribbon drawing of the restrained minimized mean structure of the MMP-1:CGS-27023A complex. The five β-strands are shown in blue, the three helices are shown in red, and the calcium (green) and zinc (purple) ions are shown as van der Waal spheres. Shown as transparent cyan is the position and shape of the S1′ pocket. The inhibitor is shown as a stick figure. The model was generated with Quanta 4.1 (Molecular Simulations, Inc., San Diego). (B) Expanded view of the MMP-1:CGS-27023A complex where the MMP-1 active site is shown as a solid surface with CGS-27023A shown as liquorice bonds generated using the program GRASP (*71*). Blue and red indicate positively charged and negatively charged surfaces, respectively.

disordered surface side chains (Table 3). The high quality of the MMP-1:CGS-27023A complex by NMR is also evident by the results of PROCHECK analysis and by a calculated, large negative value for the Lennard-Jones−van der Waals energy (−688 ± 13 kcal mol^{-1}). From the PROCHECK analysis, 90.6 ± 1.0 of the residues lie within the most favored region of the Ramachandran ϕ,Ψ plot, an overall *G*-factor of 0.21 ± 0.01, and a hydrogen bond energy of 0.77 ± 0.05, and only 4.5 ± 1.0 bad contacts/100 residues are consistent with a good quality structure comparable to ~1 Å X-ray structure.

The structural statistics determined for the MMP-1:CGS-27023A complex are essentially identical to the values previously determined for the inhibitor-free MMP-1 NMR structure (*1*). This result is not surprising since a majority of the restraints used in the refinement of the MMP-1:CGS-27023A complex originated from the inhibitor-free MMP-1 refinement. This similarity in the structural statistics between the inhibited and inhibitor-free MMP-1 structures indicate that the addition of CGS-27023A to the refinement does not seriously distort the MMP-1 structure. In addition, it suggest that the intermolecular NOEs observed in both the 3D ^{15}N-edit NOESY and the 3D ^{13}C-edited/^{12}C-filtered NOESY spectra are sufficient to properly define the structure of CGS-27023A in the active site. The quality of the NMR data to properly define the complex is also supported by the well-defined coordinates for CGS-27023A and the active-site residues, where the atomic rms distribution is 0.28 ± 0.08 and 0.54 ± 0.03 Å for the heavy atoms and backbone atoms, respectively.

Comparison of the MMP-1:CGS-27023A and Inhibitor-Free MMP-1 NMR Structures. The overall fold of the MMP-1:CGS-27023A complex is identical to the inhibitor-free MMP-1 NMR structure. The similarity between the two structures is apparent from a comparison of the atomic rms distribution for the backbone atoms for the restrained minimized MMP-1:CGS-27023A complex and the inhibitor-free MMP-1 NMR structure where the rms difference corresponds to 0.48 Å. The rms difference between the structures is within the rms distribution for the ensemble of structures calculated for the MMP-1:CGS-27023A complex, indicating that the inhibited and free structures are essentially identical within experimental error. Again, this result is not unexpected based on the methodology used to determine the structure of the MMP-1:CGS-27023A complex and given the experimental observation that a majority of the protein is unaffected by the presence of CGS-27023A.

A more interesting comparison is the observed rms difference for residues comprising the MMP-1 active site in the inhibited and free structures. In this case, the atomic rms distribution for the backbone atoms is 1.0 Å, indicating a significant difference between the two structures. It is important to note that residues P138−G144, which corresponds to an active-site dynamic loop, were not included in the overall structure comparison (*11*). This indicates that the conformation of the active-site residues and CGS-27023A are effectively determined from the experimental NOEs in the complex while the remainder of the protein is unaffected and sufficiently determined from the inhibitor-free MMP-1 restraints. The observed difference between the inhibited and free MMP-1 structures appears to correspond to a relatively uniform expansion of the active site to accommodate CGS-27023A without any significant reorganization of the structure.

As we previously reported (*11*), a surprising finding for the MMP-1:CGS-27023A complex was the observation that residues P138−G144 are highly flexible and dynamic as evident by generalized order parameters (S^2) of ≤0.6 and from the lack of NH assignments for some of these residues presumably due to exchange broadening. These results were

Table 4: Observed NOEs between CGS-27023A and MMP-1

CGS-27023A	MMP-1	NOE class	CGS-27023A	MMP-1	NOE class
HG2*	N80 Hβ1	M	3HE1	V115 Hγ2#	W
HG2*	N80 Hβ2	W	3HD1	V115 Hγ2#	M
HG2*	N80 Hα	M	3HH*	V115 Hγ2#	M
HG1*	N80 Hα	W	3HE1	H118 Hβ1	W
2HD1	N80 Hα	W	3HE1	H118 Hβ2	W
3HD1	L81 HN	W	3HH*	H118 Hβ1	M
3HD2	L81 Hγ	W	3HH*	H118 Hβ2	M
3HD1	L81 Hβ1	W	3HE1	E119 Hγ#	W
3HD2	L81 Hδ1#	M	3HH*	L135 Hδ1#	M
3HE2	L81 Hδ1#	W	3HH*	L135 Hδ2#	W
3HH*	L81 Hδ1#	W	3HH*	L135 Hα	W
3HE1	A82 HN	W	2HD2	P138 Hβ	W
3HD1	A82 HN	M	3HD2	Y137 HB#	W
1HA	A82 HN	W	3HE2	Y137 HB#	W
3HD1	A82 Hβ#	M	3HE2	S139 Hα	M
3HE1	A82 Hβ#	W	3HD2	S139 Hα	S
HG1*	H83 Hα	M	2HD2	S139 Hα	W
HG1*	H83 Hβ1	M	3HE2	Y140 Hβ2	W
HG1*	H83 Hβ2	M	3HH*	Y140 Hβ2	W
3HH*	R114 Hγ#	W	3HH*	Y140 Hϵ2	W
3HE1	V115 Hγ1#	M	3HH*	Y140 Hδ2	M
3HD1	V115 Hγ1#	W	3HH*	Y140 Hα	M
3HH*	V115 Hγ1#	W	3HD2	Y140 Hα	W
3HE1	V115 Hα	M	3HE2	Y140 Hα	S

identical for the inhibitor-free MMP-1 structure. An interesting observation from the refinement of the inhibitor-free MMP-1 structure was that, despite the lack of distance restraints, the rms distribution of the backbone atoms of these residues is less than expected when compared to the disordered N- and C-terminus (*1*). This appears to be caused by a limited amount of accessible conformational space since these residues are confined to an extended conformation by a relatively large separation (~18 Å) of the well-defined residues at each end of the dynamic-loop.

Description of the MMP-1:CGS-27023A Structure. A ribbon diagram of the restrained minimized average structure of the MMP-1:CGS-27023A is depicted in Figure 5A. The interaction of CGS-27023A in the active site of MMP-1 was determined primarily by 18 intramolecular NOEs for CGS-27023A and by a total of 48 intermolecular distance restraints between MMP-1 and CGS-27023A. Examples of the quality of the NMR spectra are shown in Figure 4, and the observed intermolecular NOEs are listed in Table 4. The key MMP-1 residues involved in the interaction with the inhibitor correspond to three distinct MMP-1 regions: residues N80, L81, A82, and H83 from β-strand IV; residues R114, V115, H118, and E119 from α-helix II; and L135, P138, Y137, S139, and Y140 from the dynamic loop (*11*). These residues comprise the S1′ and S2′ pockets of MMP-1, which is consistent with the observed chemical shift perturbations for residues 80−85, 112−124, and 134−143 (Figure 3). These results are consistent with CGS-27023A binding to the right side of the catalytic Zn. An expanded view of the fit of CGS-27023A in the S1′ and S2′ pockets of MMP-1 is shown in Figure 5B.

The interaction of CGS-27023A in the active site of MMP-1 is consistent with the observed "splayed" bound conformation determined exclusively from the intramolecular NOEs for CGS−27023A. The *p*-methoxyphenyl of CGS-27023A sits in the S1′ pocket of the MMP-1 active site. This positioning is evident from the observed NOEs from 3HH* to R114, V115, and L135, among others. The isopropyl group is in contact with H83 and N80 as evident by the strong and selective NOEs between HG1* and HG2* and the N80 and H83 side chains. Finally, the pyridine ring is essentially solvent exposed and flexible by the lack of NOEs to MMP-1. These interactions position CGS-27023A such that the hydroxamic acid moiety of CGS-27023A chelates to the "right" of the catalytic zinc and the sulfonyl oxygens are in hydrogen-bonding distance to the backbone NHs of L81 and A82. The hydrogen-bonding interaction is consistent with the large chemical shift-perturbation of the backbone NH and ^{15}N of L81 and A82.

As stated previously, the low order parameters (S^2) observed for P138−G144 in the inhibitor-free MMP-1 structure are nearly identical to the order parameters observed in the MMP-1:CGS-27023A complex, indicating that the presence of CGS-27023A does not significantly alter the dynamics of these residues in the complex. This may appear contradictory given the significant amount of NOEs observed between residues Y137−Y140 and CGS-27023A, but it is important to remember that the observed NOEs result from a time-averaged conformation. Thus, the conformation of the dynamic loop only needs to be within ≤5 Å to CGS-27023A for a fraction of the time to generate an observable NOE. Additionally, since it was previously observed (*1*) that the rms distribution for these residues in the inhibitor-free MMP-1 structure is relatively small for a flexible region, this diminishes the likelihood that the dynamic loop would be at an extreme distance (≫5 Å) from CGS-27023A. These analyses suggest that the interaction of CGS-27023A with residues Y137−Y140 is probably not a significant component of the overall binding energy of CGS-27023A with MMP-1. This is also consistent with the lack of NOEs and the solvent-exposed description of the pyridine ring. The remainder of the CGS-27023A molecule is well defined by the interaction with other residues of MMP-1, but the only residues the pyridine ring is in position to interact with are the residues in the MMP-1 dynamic loop. Therefore, the primary binding stability for CGS-27023A probably comes from the hydroxamic acid interaction with Zn, the hydrogen-bond interaction with L81-A82, the interaction of the isopropyl group with N80 and H83, and the fit of the *p*-methoxyphenyl in the S1′ pocket.

Comparison of the MMP-1 and Stromelysin:CGS-27023A Structures. There is a high structural similarity in the catalytic domain between members of the MMP family as evident by the best-fit superposition of the backbone atoms for MMP-1, stromelysin, matrilysin, and neutrophil collagenase (Figure 6A). This is consistent with the >40% sequence homology for these proteins. Despite this overall structural similarity, there exist distinct differences between these structures in the vicinity of the catalytic Zn. This is apparent by the conformational differences of the two variable loops corresponding to residues T104−Y110 and Y140−V146 in the MMP-1 sequence (Figure 6A).

The most distinct structural difference between the MMPs is the relative size and shape of the S1′ pocket. This is clearly evident by the defined S1′ pockets for MMP-1, stromelysin, matrilysin, and neutrophil collagenase depicted in Figure 6B. It is important to note that CGS-27023A was simply docked into the available X-ray structures of stromelysin, matrilysin, and neutrophil collagenase based on its complex with

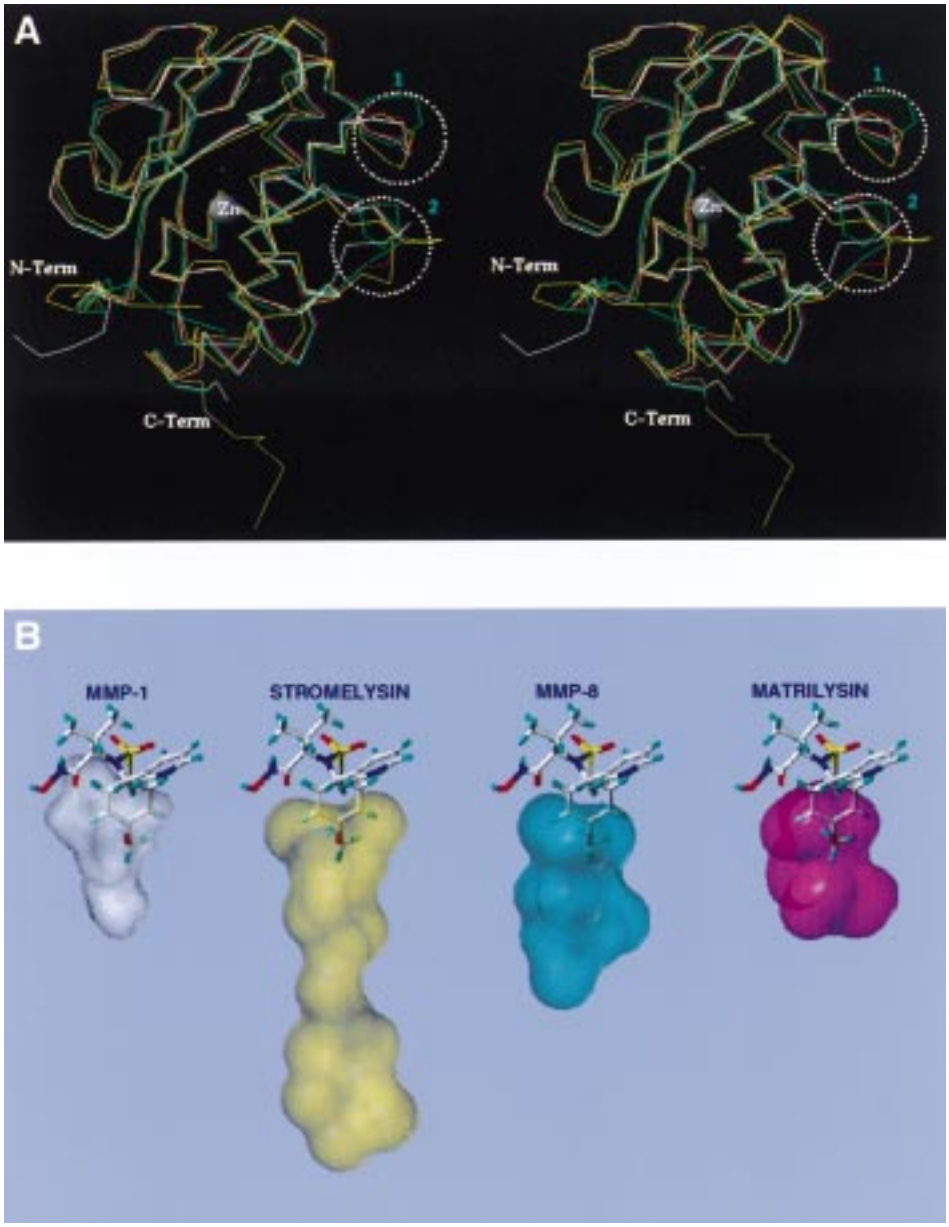

FIGURE 6: (A) The stereoview of the superposition of backbone atoms for MMP-1 (white), stromelysin (yellow), matrilysin (green), and neutrophil collagenase (red). The dotted circles indicate the variable loop regions in the vicinity of the catalytic site. Loop 1 corresponds to residues T104-Y110 and loop 2 correpsonds to residues Y140−V146 in the MMP-1 sequence. (B) The S1′ pockets of MMP-1, stromelysin, matrilysin and neutrophil collagenase with CGS-27023A docked in for comparison.

MMP-1 and is included as an aid to compare the relative size and shape of the S1′ pockets. The large difference in size in the S1′ pockets for MMP-1 and stromelysin is striking as illustrated in Figures 5B and 6B. CGS-27023A effectively fills the available S1′ pocket for MMP-1, but there is additional space available in the stromelysin S1′ pocket. In fact, the design of stromelysin inhibitors has taken advantage of this deeper S1′ pocket by using a biphenyl substituent in another series instead of the *p*-methoxyphenyl in CGS-27023A to bind into the S1′ pocket (*33*, *34*). In addition to the significant conformational difference between the S1′ pockets, there are some critical differences in the sequences between the MMPs in the active site. This difference in the amino acid composition of the MMPs active site can be dramatic, corresponding to a change from a hydrophobic residue to a charged residue which would greatly effect the nature of the interaction between the inhibitor and the protein. Therefore, in developing potent and selective inhibitors to the MMPs, these structural and sequential differences become instrumental in the design of the inhibitor.

Since an NMR structure of stromelysin complexed with CGS-27023A has been previously reported (*2*, *3*) and there is a high sequence homology (61%) (*66*) and structural similarity between the two enzymes (*1*, *2*, *18*−*20*, *22*, *24*, *26*, *27*, *29*), a direct comparison of CGS-27023A bound to both MMP-1 and stromelysin may provide insight into the specificity of MMP inhibitors and assist in the drug design process. On the basis of the observed NOEs between CGS-27023A and MMP-1, there are only two MMP-1 residues, N80 → V and R114 → L, that are involved in direct interaction with CGS-27023A which are distinct from the stromelysin active-site sequence (Table 4, Figure 7), but there is a 3-fold difference in the affinity of CGS-27023A to stromelysin and MMP-1 (12 nM versus 31 nM, respectively) (*35*).

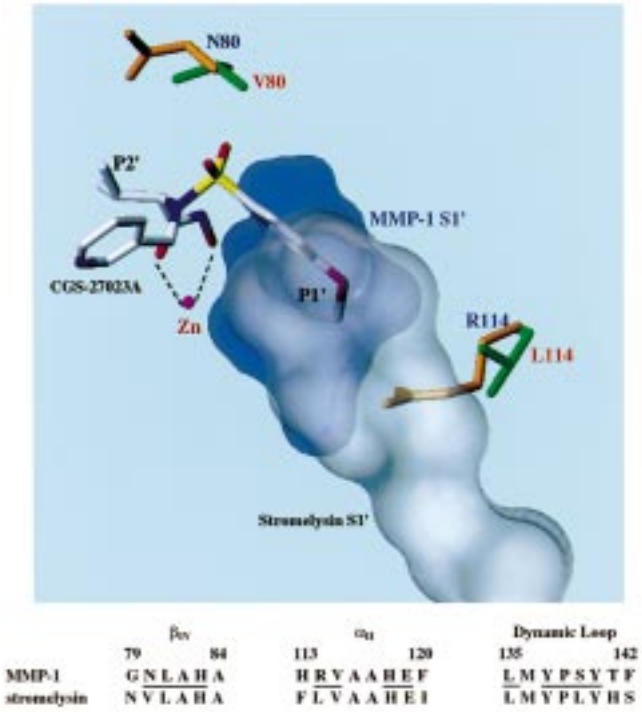

FIGURE 7: (A) A graphics view describing the protein regions of interest relative to the bound inhibitor CGS-27023A. The inhibitor, catalytic zinc, S1′ pockets of MMP-1 (blue) and stromelysin (white) and the side chains corresponding to the MMP-1:N80 (orange) → stromelysin:V80 (green) and MMP-1:R114 (orange) → stromelysin: L114 (green) differences are labeled. (B) Sequential alignment of the MMP-1 and stromelysin residues corresponding to the active site. MMP-1 residues with an observed NOE to CGS-27023A are underlined.

Examination of the stromelysin:CGS-27023A complex as reported by Gonnella et al. (1997) and Li et al. (1998) suggests a conformation generally similar to the MMP-1: CGS-27023A structure reported herein (for comparison with MMP-1, the stromelysin residue numbering was adjusted by 83). As with MMP-1, the *p*-methoxyphenyl group sits within the S1′ pocket of stromelysin based on a similar set of NOEs between 3HE*/3HD* and Y140 NH and between 3HH* and H118 NH/HD1 for stromelysin compared with the NOEs between 3HE2/3HD2 and Y140 Hα/Hβ and between 3HE1/ 3HH* and H118 Hβ for MMP-1. Similarly, both structures indicate a hydrogen bond interaction between the sulfonamide oxygens and residues L81 and A82 while the hydroxamic acid chelates the catalytic Zn.

Despite these strong similarities, the data for the MMP-1 and stromelysin complexes do suggest some subtle differences between the binding of CGS-27023A to these proteins. The most striking difference are the distinct intramolecular NOEs observed for CGS-27023A in both complexes. For MMP-1, NOEs are seen from HG1* to both 2HE1 and 2HZ. These NOEs are not observed in the stromelysin complex spectra. Conversely, NOEs between 3HD2 and 2HD1/2HD2 are observed in the stromelysin complex and not in the MMP-1 complex. These observations suggest a stronger interaction of the isopropyl group with the pyridine ring in the MMP-1 conformation compared with a stronger interaction between the *p*-methoxyphenyl and the pyridine ring in the stromelysin conformation. This may account for the observed difference in the chemical shift assignments for 2HB1/2HB2 between the MMP-1 and stromelysin complex by affecting the relative position of 2HB1/2HB2 with the *p*-methoxyphenyl group.

Similarly, there are differences in the observed intermolecular NOEs between MMP-1 and stromelysin. In MMP-1, NOEs are observed between the isopropyl methyls and the backbone and side-chain atoms of N80 and H83, while the backbone and side-chain atoms of A82 interact with the *p*-methoxyphenyl group. Conversely, in stromelysin, A82 interacts with the isopropyl methyl group in addition to the *p*-methoxyphenyl group. Additionally, an NOE is seen between the pyridine ring and L81 in stromelysin where the only NOEs to the pyridine ring in MMP-1 is to P138 and S139.

These differences suggest a distinct orientation in the positioning of CGS-27023A relative to βIV for MMP-1 compared to stromelysin, consistent with the observed difference in the HG1*/HG2* assignment for CGS-27023A complexed to MMP-1 and stromelysin, since the isopropyl methyl groups would be in distinct environments. This subtle difference in the orientation of CGS-27023A is probably attributed to the sequence difference between MMP-1 and stromelysin, where N80 in MMP-1 is replaced by valine in stromelysin. It appears that the bulkier valine side chain may rotate the isopropyl group and the pyridine ring closer to βIV as evident by the NOEs to A82 and L81, respectively. Additionally, the hydrophobic valine side chain probably provides a better interaction with the isopropyl and pyridine ring then the polar N80 side chain. The replacement of the nonpolar V80 in stromelysin by the polar N80 side chain in MMP-1 would also contribute to the observed HG1*/HG2* chemical shift differences.

Molecular graphics analysis comparing the 3D NMR structures of the MMP-1:CGS-27023A complex with a stromelysin−inhibitor complex [2SRT (*18*), the coordinates for the stromelysin:CGS-27023A complex were not available] was carried out to examine the regions in the S1′ pockets of both enzymes where the amino acid side chain differences, N80 → V and R114 → L, occur. Figure 7 depicts the protein regions of interest relative to the MMP-1-bound inhibitor where the inhibitor, catalytic zinc, S1′ pockets of MMP-1 (blue) and stromelysin (white), and the side chains corresponding to the MMP-1:N80(orange) → stromelysin: V80 (green) and MMP-1:R114 (orange) → stromelysin:L114 (green) differences are labeled. It is apparent that the S1′ pocket of MMP-1 (blue) has limited space due to the larger R114 side chain, whereas in stromelysin, the smaller L114 side chain results in an extension of the S1′ pocket (white). Examination of the inhibitor's P1′ group (*p*-methoxyphenyl group) shows that it lies within the intersection of both S1′ pockets, thus, changes in the proteins at position 114 may not contribute to the observed K_i difference. Examination of the inhibitors isopropyl group (P2′ group) shows that it comes into contact with the solvent-exposed S2′ region of both enzymes. In Figure 7, the changes between the two enzymes are MMP-1:N80 (orange) → stromelysin:V80 (green) where the N80 side chain is polar and the V80 side chain is nonpolar. Analysis of the enzymes S2′ regions suggests that this interaction is consistent with the observed potency difference since the isopropyl group of the inhibitor would form a more favorable interaction with the nonpolar V80 of stromelysin rather than the polar N80 side chain of MMP-1.

CONCLUSION

The studies described herein present the solution structure of MMP-1 complexed with a sulfonamide derivative of a hydroxamic acid compound (CGS-27023A). The structure was based on distance restraints from X-filtered NOESY experiments in conjunction with the restraints from the refinement of the inhibitor-free MMP-1 NMR structure. The inhibitor was found to bind to the "right" side of the catalytic Zn such that the *p*-methoxyphenyl ring sits in the S1′ pocket, the isopropyl moiety interacts with N80 and H83 of βIV, hydrogen bond interactions exist between the sulfonamide oxygens with residues L81 and A82, and the hydroxamic acid chelates the catalytic Zn. This inhibitor binds similarly to stromelysin, but some subtle differences in the relative orientation of CGS-27023A in the active site might be attributed to the sequence difference between MMP-1 and stromelysin.

REFERENCES

1. Moy, F. J., Chanda, P. K., Cosmi, S., Pisano, M. R., Urbano, C., Wilhelm, J., and Powers, R. (1998) *Biochemistry 37*, 1495−1504.
2. Gonnella, N. C., Li, Y.-C., Zhang, X., and Paris, C. G. (1997) *Bioorg. Med. Chem. 5*, 2193−2201.
3. Li, Y.-C., Zhang, X., Melton, R., Ganu, V., and Gonnella, N. C. (1998) *Biochemistry 37*, 14048−14056.
4. Lam, P. Y. S., Jadhav, P. K., Eyermann, C. J., Hodge, C. N., Ru, Y., Bacheler, L. T., Meek, O. M. J., and Rayner, M. M. (1994) *Science 263* (5145), 380−384.
5. Tummino, P. J., Prasad, J. V. N. V., Ferguson, D., Nouhan, C., Graham, N., Domagala, J. M., Ellsworth, E., Gajda, C., and Hagen, S. E., et al. (1996) *Bioorg. Med. Chem. 4*, 1401−1410.
6. Chrusciel, R. A., and Romines, K. R. (1997) *Expert Opin. Ther. Pat. 7*, 111−121.
7. Whittle, P. J., and Blundell, T. L. (1994) *Annu. Rev. Biophys. Biomol. Struct. 23*, 349−375.
8. Blundell, T. L. (1996) *Nature (Suppl.) 384*, 23−26.
9. Chen, J. M., Xu, S. L., Wawrzak, Z., Basarab, G. S., and Jordan, D. B. (1998) *Biochemistry 37*, 17735−17744.
10. Gronenborn, A. M., and Clore, G. M. (1995) *Crit. Rev. Biochem. Mol. Biol. 30*, 351−385.
11. Moy, F. J., Pisano, M. R., Chanda, P. K., Urbano, C., Killar, L. M., Sung, M.-L., and Powers, R. (1997) *J. Biomol. NMR 10*, 9−19.
12. Woessner, J. F., Jr. (1991) *FASEB J. 5*, 2145−2154.
13. Ries, C., and Petrides, E. (1995) *Biol. Chem. Hoppe-Seyler 376*, 345−355.
14. Browner, M. F. (1995) *Perspect. Drug Discovery Des. 2*, 343−351.
15. Morphy, J. R., Millican, T. A., and Porter, J. R. (1995) *Curr. Med. Chem. 2*, 743−762.
16. Zask, A., Levin, J. I., Killar, L. M., and Skotnicki, J. S. (1996) *Curr. Pharm. Des. 2*, 624−661.
17. Bode, W., Reinemer, P., Huber, R., Kleine, T., Schnierer, S., and Tschesche, H. (1994) *EMBO J. 13*, 1263−1269.
18. Gooley, P. R., O'Connell, J. F., and Marcy, A. I. (1994) *Nat. Struct. Biol. 1*, 111−118.
19. Lovejoy, B., Cleasby, A., Hassell, A. M., Longley, K., Luther, M., A., Weigl, D., McGeehan, G., McElroy, A. B., Drewry, D., Lambert, M. H., and Jordan, S. R. (1994) *Science 263*, 375−377.
20. Spurlino, J. C., Smallwood, A. M., Carlton, D. D., Banks, T. M., Vavra, K. J., Johnson, J. S., Cook, E. R., Falvo, J., and Wahl, R. C., et al. (1994) *Proteins: Struct., Funct., Genet. 19*, 98−109.
21. Stams, T., Spurlino, J. C., Smith, D. L., Wahl, R. C., Ho, T. F., Qoronfleh, M. W., Banks, T. M., and Rubin, B. (1994) *Nat. Struct. Biol. 1*, 119−123.
22. Becker, J. W., Marcy, A. I., and Rokosz, L. L. (1995) *Protein Sci. 4*, 1966−1976.
23. Gonnella, N. C., Bohacek, R., Zhang, X., Kolossvary, I., Paris, C. G., Melton, R., Winter, C., Hu, S.-I., and Ganu, V. (1995) *Proc. Natl. Acad. Sci. U.S.A. 92*, 462−466.
24. Van Doren, S. R., Kurochkin, A. V., Hu, W., Ye, Q.-Z., Johnson, L. L., Hupe, D. J., and Zuiderweg, E. R. P. (1995) *Protein Sci. 4*, 2487−2498.
25. Botos, I., Scapozza, L., Zhang, D., Liotta, L. A., and Meyer, E. F. (1996) *Proc. Natl. Acad. Sci. U.S.A. 93*, 2749−2754.
26. Broutin, I., Arnoux, B., Riche, C., Lecroisey, A., Keil, B., Pascard, C., and Ducruix, A. (1996) *Acta Crystallogr., Sect. D 52*, 380−392.
27. Gooley, P. R., O'Connell, J. F., Marcy, A. I., Cuca, G. C., Axel, M. G., Caldwell, C. G., Hagmann, W. K., and Becker, J. W. (1996) *J. Biomol. NMR 7*, 8−28.
28. Betz, M., Huxley, P., Davies, S. J., Mushtaq, Y., Pieper, M., Tschesche, H., Bode, W., and Gomis-Rueth, F. X. (1997) *Eur. J. Biochem. 247*, 356−363.
29. Lovejoy, B., Hassell, A. M., and Luther, M. A. (1994) *Biochemistry 33*, 8207−8217.
30. Birkedal-Hansen, H., Moore, W. G. I., Bodden, M. K., Windsor, L. J., Birkedal-Hansen, B., DeCarlo, A., and Engler, J. A. (1993) *Crit. Rev. Oral Biol. Med. 4*, 197−250.
31. Ghose, A. K., Logan, M. E., Treasurywala, A. M., Wang, H., Wahl, R. C., Tomczuk, B. E., Gowravaram, M. R., Jaeger, E. P., and Wendoloski, J. J. (1995) *J. Am. Chem. Soc. 117*, 4671−4682.
32. Rockwell, A., Melden, M., Copeland, R. A., Hardman, K., Decicco, C. P., and DeGrado, W. F. (1996) *J. Am. Chem. Soc. 118*, 10337−10338.
33. Hajduk, P. J., Sheppard, G., Nettesheim, D. G., Olejniczak, E. T., Shuker, S. B., Meadows, R. P., Steinman, D. H., Carrera, G. M., Jr., Marcotte, P. A., Severin, J., Walter, K., Smith, H., Gubbins, E., Simmer, R., Holzman, T. F., Morgan, D. W., Davidsen, S. K., Summers, J. B., and Fesik, S. W. (1997) *J. Am. Chem. Soc. 119*, 5818−5827.
34. Olejniczak, E. T., Hajduk, P. J., Marcotte, P. A., Nettesheim, D. G., Meadows, R. P., Edalji, R., Holzman, T. F., and Fesik, S. W. (1997) *J. Am. Chem. Soc. 119*, 5828−5832.
35. MacPherson, L. J., Bayburt, E. K., Capparelli, M. P., Carroll, B. J., Goldstein, R., Justice, M. R., Zhu, L., Hu, S.-I., Melton, R. A., Fryer, L., Goldberg, R. L., Doughty, J. R., Spirito, S., Blancuzzi, V., Wilson, D., O'Byrne, E. M., Ganu, V., and Parker, D. T. (1997) *J. Med. Chem. 40*, 2525−2532.
36. Piotto, M., Saudek, V., and Sklenar, V. (1992) *J. Biomol. NMR 2*, 661−665.
37. Grzesiek, S., and Bax, A. (1993) *J. Am. Chem. Soc 115*, 12593−12594.
38. Marion, D., Ikura, M., Tschudin, R., and Bax, A. (1989) *J. Magn. Reson 85*, 393−399.
39. Marion, D., Driscoll, P. C., Kay, L. E., Wingfield, P. T., Bax, A., Gronenborn, A. M., and Clore, G. M. (1989) *Biochemistry 28*, 6150−6156.
40. Zuiderweg, E. R. P., and Fesik, S. W. (1989) *Biochemistry 28*, 2387−2391.
41. Grzesiek, S., and Bax, A. (1992) *J. Am. Chem. Soc 114*, 6291−6293.
42. Grzesiek, S., Anglister, J., and Bax, A. (1993) *J. Magn. Reson., Ser. B 101*, 114−119.
43. Vuister, G. W., and Bax, A. (1993) *J. Am. Chem. Soc. 115*, 7772−7777.
44. Kay, L. E., Ikura, M., Tschudin, R., and Bax, A. (1990) *J. Magn. Reson. 89*, 496−514.
45. Moy, F. J., Seddon, A. P., Boehlen, P., and Powers, R. (1996) *Biochemistry 35*, 13552−13561.
46. Petros, A. M., Kawai, M., Luly, J. R., and Fesik, S. W. (1992) *FEBS Lett. 308*, 309−314.
47. Gemmecker, G., Olejniczak, E. T., and Fesik, S. W. (1992) *J. Magn. Reson. 96*, 199−204.
48. Ikura, M., and Bax, A. (1992) *J. Am. Chem. Soc. 114*, 2433−2440.
49. Lee, W., Revington, M. J., Arrowsmith, C., and Kay, L. E. (1994) *FEBS Lett. 350*, 87−90.

50. Delaglio, F., Grzesiek, S., Vuister, G. W., Zhu, G., Pfeifer, J., and Bax, A. (1995) *J. Biomol. NMR 6*, 277−293.
51. Garrett, D. S., Powers, R., Gronenborn, A. M., and Clore, G. M. (1991) *J. Magn. Reson. 95*, 214−220.
52. Zhu, G., and Bax, A. (1992) *J. Magn. Reson. 100*, 202−207.
53. Williamson, M. P., Havel, T. F., and Wuethrich, K. (1985) *J. Mol. Biol 182*, 295−315.
54. Clore, G. M., Nilges, M., Sukumaran, D. K., Bruenger, A. T., Karplus, M., and Gronenborn, A. M. (1986) *EMBO J. 5*, 2729−2735.
55. Wuthrich, K., Billeter, M., and Braun, W. (1983) *J. Mol. Biol. 169*, 949−961.
56. Nilges, M., Gronenborn, A. M., Bruenger, A. T., and Clore, G. M. (1988) *Protein Eng. 2*, 27−38.
57. Clore, G. M., Appella, E., Yamada, M., Matsushima, K., and Gronenborn, A. M. (1990) *Biochemistry 29*, 1689−1696.
58. Brunger, A. T. (1993) *X-PLOR Version 3.1 Manual*, Yale University, New Haven, CT.
59. Garrett, D. S., Kuszewski, J., Hancock, T. J., Lodi, P. J., Vuister, G. W., Gronenborn, A. M., and Clore, G. M. (1994) *J. Magn. Reson., Ser. B 104*, 99−103.
60. Kuszewski, J., Qin, J., Gronenborn, A. M., and Clore, G. M. (1995) *J. Magn. Reson., Ser. B 106*, 92−96.
61. Kuszewski, J., Gronenborn, A. M., and Clore, G. M. (1996) *Protein Sci. 5*, 1067−1080.
62. Kuszewski, J., Gronenborn, A. M., and Clore, G. M. (1997) *J. Magn. Reson. 125*, 171−177.
63. Kleywegt, G. J., and Jones, T. A. (1997) *Methods Enzymol. 277*, 208−230.
64. Browner, M. F., Smith, W. W., and Castelhano, A. L. (1995) *Biochemistry 34*, 6602.
65. Chen, J. M., Sheldon, A., and Pincus, M. R. (1995) *J. Biomol. Struct. Dyn. 12*, 1129−1159.
66. Whitham, S. M., Murphy, G., Angel, P., Rahmsdorf, H. J., Smith, B. J., Lyons, A., Harris, T. J. R., Reynolds, J. J., Herrlich, P., and Docherty, A. J. P. (1986) *Biochem. J. 240*, 913−916.
67. Brooks, B. R., Bruccoleri, R. E., Olafson, B. D., States, D. J., Swaminathan, S., and Karplus, M. (1983) *J. Comput. Chem. 4*, 187−217.
68. Nilges, M., Clore, G. M., and Gronenborn, A. M. (1988) *FEBS Lett. 239*, 129−136.
69. Nilges, M., Clore, G. M., and Gronenborn, A. M. (1988) *FEBS Lett. 229*, 317−324.
70. Laskowski, R. A., MacArthur, M. W., Moss, D. S., and Thornton, J. M. (1993) *J. Appl. Crystallogr. 26*, 283−291.
71. Nicholls, A., Sharp, K., and Honig, B. (1991) *Proteins: Struct., Funct., Genet. 11*, 281ff.

BI982576V